Structural Changes upon Photoexcitation into the Metal-to-Ligand Charge-Transfer State of $[Cu(pqx)(PPh_3)_2]^+$ Probed by Resonance Raman Spectroscopy and Density Functional Theory

Mark R. Waterland,*,† Sarah L. Howell,‡ Keith C. Gordon,*,‡ and Anthony K. Burrell§

MacDiarmid Institute for Advanced Materials and Nanotechnology, Institute of Fundamental Sciences, Massey University, Palmerston North, New Zealand, MacDiarmid Institute for Advanced Materials and Nanotechnology, Department of Chemistry, University of Otago, P.O. Box 56, Dunedin, New Zealand, and Los Alamos National Laboratory, P.O. Box 1663, Los Alamos, New Mexico 87545

Received: June 2, 2005; In Final Form: August 4, 2005

The structural changes that occur when $[Cu(pqx)(PPh_3)_2]^+$ (pqx is 2-(2′-pyridyl)quinoxaline) undergoes excitation through a metal-to-ligand charge-transfer (MLCT) transition are investigated using resonance Raman excitation profiles coupled with density functional theory (DFT). The DFT calculations predict bond lengths to within 3 pm and absolute deviations of 7 cm^{-1} for the vibrational frequencies of $[Cu(pqx)(PPh_3)_2]^+$. TD-DFT calculations of oscillator strengths ($f = 0.089$) and band positions (419 nm) showed close agreement with experiment ($f = 0.07$, 431 nm). Resonance Raman spectra show the 527 cm^{-1} (ν_{29}) and 1476 cm^{-1} (ν_{75}) modes undergo the largest dimensionless displacement ($\Delta = 1.5$ and 1.1, respectively) following photoexcitation into the MLCT Franck−Condon region. The solvent couples strongly to the MLCT transition and resonance Raman intensity analysis (RRIA) gives a solvent reorganization energy of 3400 cm^{-1} for dichloromethane and 2800 cm^{-1} for chloroform solutions. A large inner-sphere reorganization of 3430 cm^{-1} in dichloromethane solution (3520 cm^{-1} in chloroform solution) was found for $[Cu(pqx)(PPh_3)_2]^+$, indicating that the molecule as a whole undergoes significant distortion following MLCT excitation.

I. Introduction

Transition metals of low oxidation state form complexes with strong π-acceptor ligands, such as bipyridyl and phenanthroline, that exhibit intense metal-to-ligand charge-transfer (MLCT) transitions. The resulting MLCT states are often emissive and can be generated optically or electrochemically, with electrochemical generation resulting in electroluminescence. The electroluminescence of metal-based complexes has attracted considerable attention recently in their application to organic light emitting diodes.[1−7] Metal polypyridyl complexes have also found utility in solar energy systems. Hole and electron transfer are key processes in the operation of organic light emitting diodes and solar cells.[8−12] Considering the diode as a solid solution of emissive solute molecules in a polymer solvent, the charge-transfer processes leading to electroluminescence may be considered within the framework of the Marcus−Hush theory.[13] To maximize the rates of these processes, the total reorganization energy needs to be minimzed. For inner-sphere reorganization this corresponds to minimizing the structural distortions accompanying charge transfer.

One approach to measuring the reorganization energy of charge-transfer processes of metal polypyridyl systems is to use an optical probe of a photoinduced charge-transfer process. The optical response of a system undergoing a charge-transfer process involves the same material response as a system undergoing thermally driven electron or hole transfer.[14] Resonance Raman spectroscopy is a powerful optical probe of charge-transfer processes.[15] Mode-specific reorganization energies (whose sum gives the total nuclear reorganization energy) are determined from the integrated intensity of the corresponding band in the Raman spectrum, and the solvent reorganization is obtained from the magnitudes of the resonance Raman intensities and the linear absorption line shape. These contributions may be determined independently provided absolute resonance Raman intensities are measured and the absorption and Raman data are modeled simultaneously.

The resonance Raman intensities are determined in part by the displacement along each vibrational mode that translates the ground-state geometry into the geometry of the resonantly excited state. Qualitatively, the mode displacements will be determined by differences in electron density between the ground and excited state for a given mode. Thus the Raman intensities allow the structural changes following photoexcitation to be determined. However, the structural changes determined by an analysis of the resonance Raman intensities is given in terms of dimensionless displacements (Δ) along the normal modes whereas bond length and bond angle changes are perhaps the more natural coordinate system.[16−20] A normal coordinate analysis provides the link between the normal modes and bond lengths and angles. With the increase in computing resources and the development of density functional theory (DFT), normal coordinate analyses of transition metal complexes are now possible. One of the first examples of a study of metal complexes was that of Pulay et al.[21] They used DFT implemented with the hybrid B3LYP functional and a mixed basis set comprising the standard 6-31G* basis on C, O, and H and Ahlrichs' valence triple-ζ (VTZ) on the metal atoms to examine

* Corresponding authors. E-mail: M.R.W., M.Waterland@massey.ac.nz; K.C.G., kgordon@alkali.otago.ac.nz.
† Massey University.
‡ University of Otago.
§ Los Alamos National Laboratory.

10.1021/jp052954n CCC: $30.25
Published on Web 09/10/2005

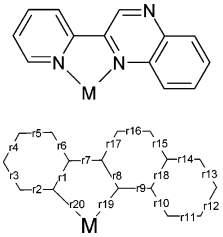

Figure 1. Structure and bond labeling for $[Cu(pqx)(PPh_3)_2]^+$, M = $\{Cu(PPh_3)_2\}^+$.

the structure and vibrational (IR) spectra of a series of trivalent metal trisacetylacetonate complexes. In a series of papers Zheng et al. have used DFT to examine the electronic properties of Fe, Ru, and Os polypyridyl complexes.[22−28] In these papers the primary focus has been on the nature of the frontier molecular orbitals present in such complexes. More recently, frequency calculations have been used to interpret the spectroscopic data for the MLCT excited state of $[Re(bpy)(CO)_3(4\text{-Etpy})]^+$ (bpy = 2,2′-bipyridine, 4-Etpy = 4-ethylpyridine) using DFT (B3LYP), with a modified LANL2 basis set for the effective core potential of the Re(I) center and a 6-31G* basis set for the other atoms. From this study the symmetries and normal vibrational modes for the carbonyl stretches have been established.[29−31] These studies focus on the vibrational bands due to the CO modes; however, it is also possible to model the vibrational spectra of the ligands associated with the metal complexes. This is pertinent to this study as the distortions of the *ligand* upon photoexcitation are probed through resonance Raman excitation profile measurements. Computational studies on the complexes containing ligands such as 1,10-phenanthroline (phen) have been carried out by a number of groups. Howell et al.[32] examined the vibrational spectra of $[Cu(phen)(PPh_3)_2]^+$ and that of the corresponding complex with perdeuterated phen and the reduced complexes of both. They found that the structure of the complex could be well modeled using B3LYP/6-31G(d). The calculated structure and that determined by X-ray crystallography differed by 0.02 Å in bond lengths. For the vibrational data the mean absolute deviation between experimental and calculated data was 10 cm^{-1}.

In this paper we present the resonance Raman and absorption spectra of a copper(I) polypyridyl complex, $[Cu(pqx)(PPh_3)_2]^+$ (pqx is 2-(2′-pyridyl)quinoxaline) in solution (Figure 1). We present a resonance Raman intensity analysis (RRIA) and extract dimensionless displacements, mode-specific reorganization energies, and solvent reorganization energies associated with the charge-transfer transition. We present results from DFT calculations of the vibrational normal modes and nonresonant intensities and use the normal modes to interpret the output from the RRIA.

II. Experimental Section

$[Cu(pqx)(PPh_3)_2]BF_4$ was prepared from $[Cu(CH_3CN)_2(PPh_3)_2]BF_4$ on the basis of literature methods.[33] $[Cu(CH_3CN)_2(PPh_3)_2]BF_4$ was synthesized on the basis of literature procedures.[34]

$Cu(BF_4)_2 \cdot xH_2O$ (0.715 g) and excess copper metal were added to argon-purged acetonitrile (100 mL), and the mixture was stirred for 2 h. The excess copper metal was removed by filtration. The filtrate was rotary evaporated. A 2 mol equiv sample of PPh_3 was added with acetonitrile (100 mL), and the solution was refluxed for 3 h. The solvent was then removed by rotary evaporation. $[Cu(CH_3CN)_2(PPh_3)_2]BF_4$ was recrystallized from dichloromethane. The ligand, pqx (0.020 g, 0.097 mmol), in chloroform (100 mL) was added to $[Cu(CH_3CN)_2(PPh_3)_2]BF_4$ (0.073, 0.097 mmol) in chloroform (100 mL), and the mixture was stirred for 30 min under an argon atmosphere. The solvent was removed by rotary evaporation, and $[Cu(pqx)(PPh_3)_2]BF_4$ was purified by recrystallization from methanol.

$[Cu(pqx)(PPh_3)_2]BF_4$. Yield: 61%. Found: C, 66.04; H, 4.39; N, 4.57. Calcd for $[Cu(pqx)(PPh_3)_2]BF_4 \cdot {}^2/_3CH_3OH$: C, 66.02; H, 4.65; N, 4.65; ^1H NMR ($CDCl_3$, 300 MHz): δ 9.79 (s, 1H), 8.74 (d, 1H), 8.38−8.28 (m, 2H), 8.16 (d, 1H), 7.88 (br, 1H), 7.45 (dd, 1H), 7.57 (br, 1H), 7.4−7.1 (m, 31H).

Spectroscopic grade solvents were used for all spectroscopic measurements. ^1H NMR spectra were recorded at 25 °C, using either a Varian 300 MHz NMR spectrometer. Chemical shifts are given relative to residual solvent peaks. Microanalyses were performed at the Campbell Microanalysis Laboratory at the University of Otago. FT-IR spectra were collected, using a Perkin-Elmer Spectrum BX FT-IR system with Spectrum v.2.00 software, of potassium bromide (KBr) disks. Spectra were measured using 64 scans. Band positions are reproducible within 1−2 cm^{-1}. FT-Raman spectra were collected on powder samples, using a Bruker Equinox-55 FT-interferometer bench equipped with an FRA/106 Raman accessory and utilizing OPUS (version 5.0) software. An Nd:YAG laser with 1064 nm excitation wavelength was used. An InGaAs diode (D424) operating at room temperature was used to detect Raman photons. Spectra were typically measured using 16 scans at a power of 100 mW and a resolution of 4 cm^{-1}.

A continuous-wave Innova I-302 krypton-ion laser (Coherent, Inc.) or Melles Griot Omnichrome MAP-543 argon-ion laser was used to generate resonance Raman scattering. Band-pass filters removed the Kr^+ plasma emission lines from the laser output. The laser output was adjusted to give between 15 and 20 mW at the sample. The incident beam and the collection lens were arranged in a 135° backscattering geometry to reduce Raman intensity reduction by self-absorption.[35] An aperture-matched lens was used to focus scattered light through a narrow band line-rejection (notch) filter (Kaiser Optical Systems) and a quartz wedge (Spex) and onto the 100 μm entrance slit of a spectrograph (Acton Research SpectraPro 500i). The collected light was dispersed in the horizontal plane by a 1200 grooves/mm ruled diffraction grating (blaze wavelength 500 nm) and detected by a liquid nitrogen cooled back-illuminated Spec-10: 100B CCD controlled by a ST-133 controller and WinSpec/32 (version 2.5.8.1) software (Roper Scientific, Princeton Instruments).

Wavenumber calibration was performed using Raman bands from a 1:1 (by volume) mixture of acetonitrile and toluene sample.[36,37] Peak positions were reproducible to within 1−2 cm^{-1}. Spectra were obtained with a resolution of 5 cm^{-1}. Freshly prepared samples were held in a spinning NMR tube. The concentration of the solute was 5 mmol dm^{-3}. Spectral intensities were corrected for self-absorption,[38] differential band-pass, and throughput of the spectrograph and detector sensitivity. Integrated band intensities were obtained using the peak fitting module in Origin Pro 7.5. Solute Raman cross-sections were obtained relative to the 702/740 cm^{-1} doublet of dichloromethane[39] and the 666 cm^{-1} band in chloroform.[40]

Electronic absorption spectra were recorded on a Varian Cary 500 scan UV−vis−NIR spectrophotometer, with Cary WinUV software. Samples were typically $\sim 10^{-4}$ mol dm^{-3}.

Simulations. The absorption and resonance Raman intensities were simulated using the time-dependent formulation originally developed by Lee and Heller[41,42] and summarized by Myers.[43] The Raman amplitude between the initial and final vibrational states, α_{if}, is calculated as the half-Fourier transform of the time-dependent overlap of a wave packet propagating on the resonant

electronic excited and the $v'' = 1$ ground-electronic-state vibrational wave function:

$$\alpha_{if}(\omega_L,\delta) = \frac{1}{\hbar}\int_0^\infty dt\, \langle \chi_f|\chi_i(t)\rangle \exp[i(\omega_L - \omega - \delta + \omega_i)t - g(t)]$$

where ω_L is the incident laser frequency, $\hbar\omega_i$ is the energy of the initial vibrational level (set to zero as scattering from all modes in the simulation occurs from the ground vibrational level), ω is the zero-zero electronic transition frequency, and δ is the electronic zero-zero frequency shift due to inhomogeneous broadening. $\langle c_f| = \langle f|\mu_0$ and $\langle c_i| = \langle i|\mu_0$ are the multidimensional ground-state vibrational wave functions multiplied by the transition dipole moment, and $|\chi_i(t)\rangle = \exp(-iHt/\hbar)|\chi_i\rangle$ is the initial vibrational wave function propagated for a time, t, on the electronic excited-state surface, by the excited-state vibrational Hamiltonian. $g(t)$ is the solvent broadening function modeled as an overdamped Brownian oscillator.[14] Separable harmonic oscillators, with frequencies taken from the ground-state Raman modes were used in the model for the potential energy surfaces. The ground- and excited-state normal modes are assumed to have the same form, i.e., Dushinsky rotation is not included, and non-Condon effects were not included.

The experimental observable, the differential Raman cross-section, is calculated via

$$\left(\frac{d\sigma}{d\Omega}\right)_{||+\perp} = \sum_i B_i \sum_f \int d\omega_S \left(\frac{{\omega_S}^3\omega_L}{c^4}\int_{-\infty}^{+\infty} d\delta\, G(\delta)\left|\alpha_{if}(\omega_L,\delta)\right|^2\right) L_{if}(\omega_L - \omega_S)$$

where B_i is the Boltzmann population of the initial vibrational state (assumed to be unity here) and $L_{if}(\omega_L-\omega_S)$ is a Raman line-shape function. $G(\delta)$ is a normalized inhomogeneous broadening function which is taken to be Gaussian.

The absorption cross-section is calculated at the same level of theory using

$$\sigma_A(\omega) = \frac{4\pi|\mu|^2\omega}{3n\hbar c}\sum_i B_i \int_{-\infty}^{+\infty} d\delta\, G(\delta)\, \mathrm{Re}\int_{-\infty}^{+\infty} dt\, \langle \chi_i|\chi_i(t)\rangle \exp[i(\omega_L - \omega - \delta + \omega_i)t - g(t)]$$

where the real part of the Fourier transform is taken and n is the refractive index of the solvent.

Ab Initio Calculations. The geometry, vibrational frequencies, and their IR and Raman intensities were calculated using DFT calculations (B3LYP functional) with a 6-31G(d) basis set. These were implemented with the Gaussian 03W[44] program package. The visualization of the vibrational modes was provided by the Molden package[45] and GaussViewW (Gaussian Inc.). Frequency calculations on the complexes produced no imaginary frequencies, indicating that in each case the minimum energy point was located. The Raman intensities are calculated from the Raman activity for 1064 nm excitation.[46−48] The frequencies were scaled by 0.975, as this was found to give the lowest mean absolute deviation between experimental and calculated data.

III. Results

III.a. Calculated and Experimentally Determined Structure for Copper(I) Complex. To simplify the calculations on the copper complex, and because it is the pqx geometry and modes that are primarily of interest, $[Cu(pqx)(PH_3)_2]^+$ was modeled instead of $[Cu(pqx)(PPh_3)_2]^+$. The only drawback with this strategy is the predicted IR and Raman spectra contain bands associated with the PH_3 units that are not present in the experimental data. Such modes are easily identified by visualization of the modes and inspection.

TABLE 1: Calculated and Experimental Bond Lengths (Å) and Angles (deg) for $[Cu(pqx)(PPh_3)_2]^+$

	calculated	experimental
r_1	136	134
r_2	134	134
r_3	139	139
r_4	139	134
r_5	139	137
r_6	140	137
r_7	148	148
r_8	134	131
r_9	137	135
r_{10}	141	140
r_{11}	138	136
r_{12}	142	140
r_{13}	138	134
r_{14}	142	139
r_{15}	136	137
r_{16}	131	129
r_{17}	142	141
r_{18}	143	141
r_{19}	201	213
r_{20}	202	208
r_{19}-r_{20}	82	78
r_1-r_7-r_8	0	6

Selected calculated structural parameters of $[Cu(pqx)(PH_3)_2]^+$ and the crystallographic data for $[Cu(pqx)(PPh_3)_2]^+$ are shown in Table 1. The full set of parameters is available as Supporting Information. The bond lengths across the pqx ligand are calculated to within 3 pm for virtually all bonds; the exceptions are r_4 and r_{13}. The bond lengths for the copper to N linkages are underestimated in the calculation. A small twist of the ligand is also not calculated.

Veroni et al. have reported the related $Mo(CO)_4(pqx)$ complex, which shows strong solvatochromic behavior.[49] The structure of the pqx ligand in this complex is very similar to that reported herein.

III.b. Vibrational Spectra. DFT calculations are effective in predicting the structure of the $[Cu(pqx)(PH_3)_2]^+$ complex. They may also be used to calculate the vibrational (IR and Raman) spectra. This is useful for two reasons: (1) The predicted spectra may be compared to experimental data to establish the reliability of the calculations. (2) The predicted normal modes of vibration provide an indication of the structural distortion of the complexes when excited by relating them to the dimensionless displacements determined by the RRIA.

The calculated and experimental nonresonant Raman spectra, in the 450−1650 cm^{-1} region, for $[Cu(pqx)(PPh_3)_2]^+$ are shown in Figure 2. For the bands in the 1000−1650 cm^{-1} region the mean absolute deviation between experimental and calculated frequencies (postscaling by 0.975) is 7 cm^{-1}. The strongest features in the nonresonant Raman spectrum ($\lambda_{exc} = 1064$ nm) lie at 1596, 1584, 1571, 1538, 1473, 1374, 1325, and 1000 cm^{-1}. These are predicted by DFT calculation to lie at 1611 (ν_{80}), 1582 (ν_{79}), 1575 (ν_{78}), 1548 (ν_{77}), 1478 (ν_{75}), 1374 (ν_{71}), 1321 (ν_{69}), and 1009 (ν_{50}) cm^{-1}, respectively. The normal modes that describe them are pyridine-based for the 1611 (ν_{80}) and 1009 (ν_{50}) cm^{-1} predicted bands, quinoxaline-based for the predicted band at 1478 cm^{-1} (ν_{75}), and delocalized for the bands predicted

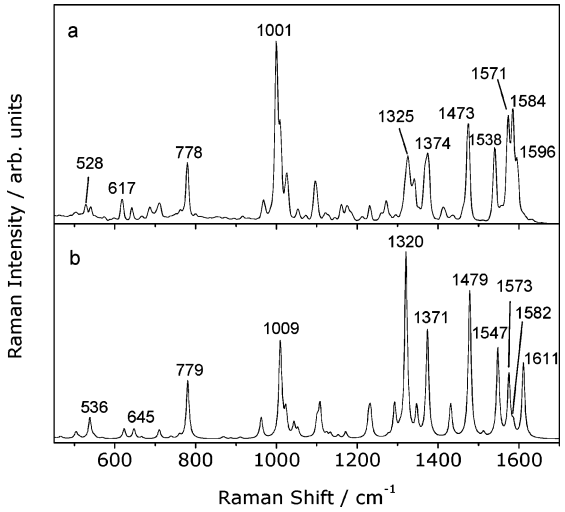

Figure 2. (a) Experimental nonresonant FT-Raman spectrum of solid-state sample of $[Cu(pqx)(PPh_3)_2](BF_4)$. (b) Calculated nonresonant Raman spectrum of $[Cu(pqx)(PH_3)_2]^+$.

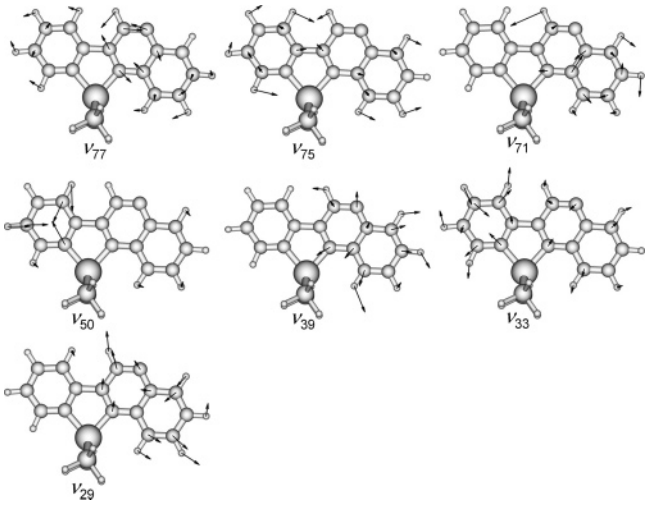

Figure 3. Selected normal modes for $[Cu(pqx)(PH_3)_2]^+$.

at 1374 (ν_{71}) and 1321 cm^{-1} (ν_{69}). The 1321 cm^{-1} is an inter-ring stretch mode. A selection of normal modes is shown in Figure 3.

III.c. Electronic Spectra. The electronic spectra for $[Cu(pqx)PPh_3)_2]^+$ contain two types of transitions in the UV/visible region: the π,π^* ligand-centered (LC) transitions at approximately 370 nm and a lower energy band at 430 nm that is attributed to a metal-to-ligand charge-transfer (MLCT) transition.

TD-DFT calculations are summarized in Table 2. The calculation for $[Cu(pqx)(PH_3)_2]^+$ predicts two transitions of reasonable intensity ($f > 0.05$) in the 350−700 nm region. A low energy transition is predicted at 419 nm with $f = 0.089$; this is an MLCT transition that is dominated by the one-electron transition between MOs 85 and 87. MO 87 (shown in Figure 4) is the LUMO (ligand π^* in character), and MO 85 is a dπ orbital. This corresponds to the observed transition at 431 nm. A second more intense transition is predicted at 328 nm ($f = 0.18$), which is made of three configurations all involving π ligand MOs and all terminating on the LUMO. This transition corresponds to the observed 348 nm band.

III.d. Resonance Raman Spectra and Simulations. The resonance Raman spectrum of $Cu(pqx)(PPh_3)_2^+$ in dichloromethane recorded with 488 nm excitation is shown in Figure 5. Experimental and simulated absolute resonance Raman cross-sections for the dichloromethane and chloroform solutions are available as Supporting Information (Table 1S and 2S, respectively).

TABLE 2: TD-DFT Calculations on $Cu(pqx)(PH_3)_2^+$ [a]

λ_{calc}/nm (f_{calc})	λ_{expt}/nm (ϵ/M^{-1} cm^{-1}; f_{expt})	configuration (coefficients)
424 (0.002)		84, 87 (0.70)
419 (0.089)	431 (3000; ***0.07***)	85, 87 (0.66)
370 (0.013)		81, 87 (−0.45)
		83, 87 (0.51)
348 (0.002)		81, 87 (0.47)
		82, 87 (0.34)
		83, 87 (0.35)
336 (0.001)		79, 87 (0.66)
		86, 88 (0.16
328 (0.183)	348 (12 000; ***0.19***)	81, 87 (−0.22)
		82, 87 (0.52)
		83, 87 (−0.20)

[a] Only transitions with appreciable f are listed.

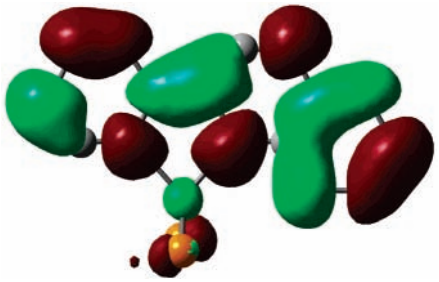

Figure 4. Pictorial representation of MO 87 LUMO.

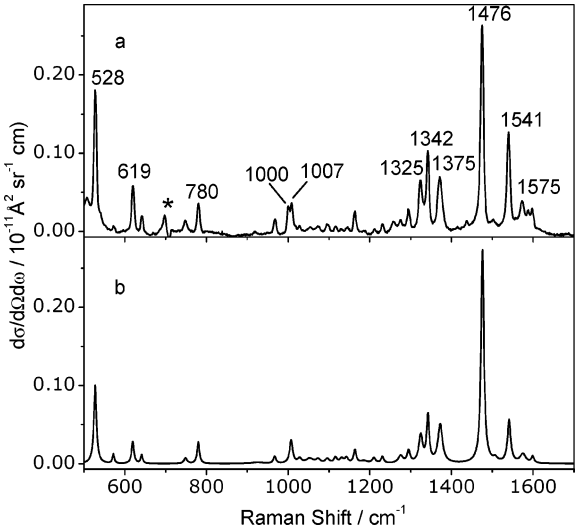

Figure 5. (a) Experimental resonance Raman spectrum for $Cu(pqx)(PPh_3)_2^+$ in dichloromethane solution. (b) Simulated spectrum. The dichloromethane solvents bands have been subtracted in the experimental spectrum. The asterisk indicates the residual from the subtraction process. The scale of the y-axis has been set by requiring the integrated band intensities to correspond to the values in the Supporting Information.

The absorption spectrum and simulated fits to the absorption spectrum are shown in Figure 6. Parameters used to generate Figure 6 are listed at the foot of Table 3. The fit to the low energy charge-transfer band is very good, due in large part to the dimensionless displacements of active vibrations being constrained by the relative resonance Raman intensities. The absolute magnitude of the Raman intensities constrains the value of the homogeneous broadening. The large homogeneous broadening of 2750 cm^{-1} in dichloromethane corresponds to a solvent reorganization energy (λ_S) of 3400 cm^{-1}, consistent with

TABLE 3: Mode Displacements and Reorganization Energies for the MLCT State of $Cu(pqx)(PPh_3)_2^+$ [a]

				dichloromethane		chloroform	
mode number	expt'l freq (cm^{-1})	calc'd freq (cm^{-1})	descriptor[b]	Δ	λ (cm^{-1})	Δ	λ (cm^{-1})
29	527	538	$0.2r_{19} + 0.15r_{10} + 0.1r_{15}$	1.5	593	1.7	762
31	572	569		0.3	31	0.3	31
32	619	623	$0.3r_{20} + 0.3r_{19}$	0.6	112	0.6	112
33	641	648		0.4	51	0.4	51
36	749	739		0.3	34	0.3	34
39	780	781	$0.3r_{18} + 0.2r_{14} - 0.3r_{19} + 0.2r_{15}$	0.5	97	0.5	97
44	925	910		0.3	29	0.3	29
47	967	962		0.3	44	0.3	44
50	1007	1009	$0.5r_{20} - 0.3r_1 - 0.2r_2 - 0.2r_6 + 0.2r_5$	0.5	126	0.5	126
52	1028	1023		0.2	21	0.2	21
54	1053	1053		0.3	47	0.3	47
55	1073	1081		0.3	34	0.3	34
56	1096	1101		0.3	34	0.3	34
59	1116	1108		0.2	22	0.2	22
60	1131	1124		0.2	18	0.2	18
61	1143	1134		0.2	23	0.2	23
62	1164	1153		0.3	52	0.3	52
63	1185	1171		0.2	24	0.2	24
64	1210	1229		0.2	14	0.2	14
65	1231	1233		0.2	25	0.2	25
66	1276	1276		0.3	57	0.3	57
68	1295	1305		0.3	58	0.3	58
69	1325	1321	$0.6r_7 - 0.3r_{16} - 0.2r_8 - 0.2r_2 + 0.2r_9$	0.5	166	0.5	166
70	1342	1347	$0.3r_8 - 0.2r_{17} + 0.2r_{16}$	0.5	168	0.5	168
71	1373	1374	$0.6r_{18} + 0.4r_{10} + 0.3r_9 - 0.3r_{11}$	0.6	247	0.6	247
75	1476	1478	$0.3r_7 - 0.3r_3 + 0.2r_8 - 0.2r_{10}$	1.1	893	1.1	893
76	1507	1512	$0.6r_{16} + 0.6r_8 + 0.4r_{15} - 0.4r_9 + 0.3r_{10}$	0.2	30	0.2	30
77	1541	1548		0.6	277	0.5	193
78	1575	1575		0.3	71	0.3	71
80	1599	1611		0.2	32	0.2	32

[a] Remaining modeling parameters for dichloromethane (chloroform) solutions: electronic origin 16 500 cm^{-1} (17 800 cm^{-1}), solvent broadening parameters $D = 2750$ cm^{-1} (2400 cm^{-1}), $\Lambda = 275$ cm^{-1} (240 cm^{-1}), $\lambda_S = 3400$ cm^{-1} (2800 cm^{-1}), transition dipole length 0.625 Å (0.650 Å), $T = 298$ K, and the inhomogeneous broadening is set to zero in both solutions. [b] Mode descriptors are given for modes with large Δ. The descriptors relate the stretch contribution for the bond lengths as labeled in Figure 1.

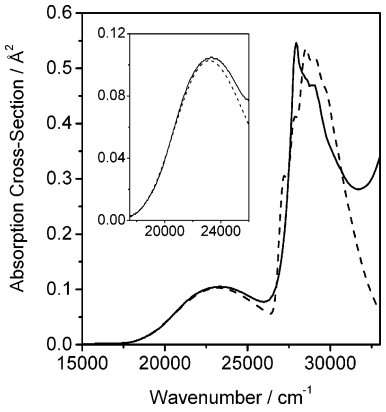

Figure 6. Experimental (solid) and simulated (dashed) absorption spectra for $Cu(pqx)(PPh_3)_2^+$ in dichloromethane solution. Inset shows MLCT band.

a simple dielectric continuum model[50] and previous resonance Raman intensity analyses.[39,51] A slightly smaller value of 2400 cm^{-1} ($\lambda_S = 2800$ cm^{-1}) for the homogeneous broadening was obtained for the chloroform solution. The angle between the transition dipole moments for the MLCT and LC transitions enters into the simulations; however, the fits are largely insensitive to this parameter. Therefore this angle was held fixed at 90°; the MLCT transition dipole lies in the metal−ligand plane roughly bisecting the inter-ring bond of the pqx ligand whereas the ligand $\pi\pi^*$ transition dipole lies along the long axis of the ligand. Under conditions where the MLCT and LC states both contribute to the Raman scattering, the depolarization ratio (ρ) can provide useful information regarding the relative orientation of the electronic transition dipole moments. When the two electronic transitions are parallel, one expects $\rho = 1/3$; for perpendicular, and equal magnitude, transitions, $\rho = 1/8$. Where only a single state contributes to the depolarization ratio, a value of $\rho = 1/3$ is also expected. The depolarization ratios for $Cu(pqx)(PPh_3)_2^+$ in dichloromethane solution were determined for three of the excitation wavelengths: 514.5, 457.9, and 406.1 nm. For 514.5 nm excitation the values of the depolarization ratios for the strongest bands in the $Cu(pqx)(PPh_3)_2^+$ spectrum were all $\rho = 1/3$, within experimental error, which is consistent with excitation into the red edge of the MLCT transition where only a single electronic state contributes to the scattering. As the excitation wavelength is shifted toward the blue edge of the MLCT transition, some modes show slight deviations from $\rho = 1/3$ to slightly higher values (0.5−0.6). Overlap of the MLCT and LC transitions is expected in this region and may be the cause of the change in the value of the depolarization ratio. However, the large uncertainty associated with the depolarization ratios prevents us from making definitive statements about the relative orientation of the LC and MLCT transition dipoles.

The fit to the ligand-centered (LC) absorption band is less satisfactory. The LC band exhibits structure that may be due to multiple electronic origins (as suggested by the TD-DFT calculations), vibronic structure from a single electronic origin, or some combination of both. In the two-state model we use a single electronic state to represent the LC band. Given the close agreement between the calculated positions and oscillator strengths for the MLCT state, we may use the TD-DFT output as a guide to the position and intensity of the LC bands. The

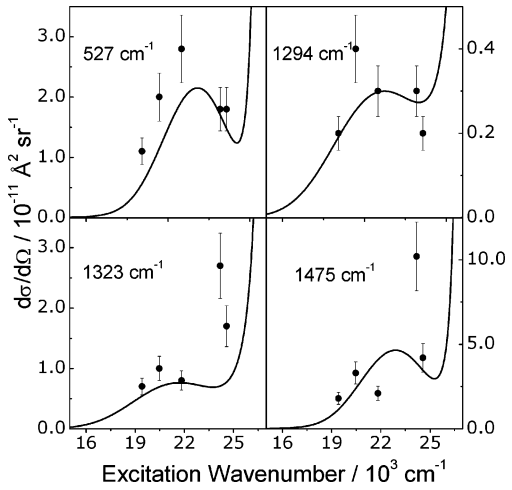

Figure 7. Selected resonance Raman excitation profiles for $Cu(pqx)(PPh_3)_2^+$ in dichloromethane. Data points are experimental points, solid curves are simulated excitation profiles.

TD-DFT output (Table 2) suggests a strong LC transition around 330 nm with intensity approximately twice that of the MLCT transition. Thus a transition dipole length of 1.0 Å and an electronic origin of 24 000 cm^{-1} were used as input parameters for the LC excited state. Similar parameters were extracted from fitting a sum of Gaussians to the absorption spectrum. Optimization resulted in an unchanged transition dipole length and a slightly modified (26 000 cm^{-1}) electronic origin. A relatively small homogeneous broadening (600 cm^{-1}) is required to fit the sharp red edge of the ligand-centered band and introduces vibronic structure into the simulated spectra. Without resonant Raman data for the LC transition, it is difficult to fit the vibronic structure in the LC band as the mode displacements parameters are largely unrestrained and highly coupled.

The resonance Raman excitation profiles are shown in Figure 7. The Raman intensities recorded with 514.5 and 488 nm excitation are closely simulated by the two-state model. Excitation on the red edge of the charge-transfer band is less likely to show interference effects from the LC band. Interference effects from higher lying electronic states may be the cause of the poor agreement for some modes between the simulated and experimental values for the Raman data excited with 406 and 413 nm excitation. Raman data on resonance with the strong LC transition would have been useful in fitting the absorption profile for the LC transition; however, strong fluorescence prevented Raman data from being acquired with UV excitation. The exact nature of the fluorescence is unclear, but possibilities include trace amounts of free ligand impurity or ligand-centered emission from the complex itself, although it should be noted that excitation into the MLCT band results in virtually no detectable emission. A plausible explanation for the emission generated with UV excitation would be emission from very small amounts of free ligand due to photodissociation.

It is interesting to compare the magnitude of the solvent (outer-sphere) reorganization energy (as determined by the homogeneous broadening) and the total inner-sphere reorganization (λ_i) determined by

$$\lambda_i = \sum_j \frac{1}{2}\omega_j \Delta_j^2$$

The solvent reorganization is approximately 3400 cm^{-1} for dichloromethane and the inner-sphere contribution to the reorganization energy for the metal-to-ligand charge transfer has an almost identical value (3430 cm^{-1}). For chloroform solution, the inner-sphere reorganization energy (3520 cm^{-1}) exceeds the solvent reorganization by more than 700 cm^{-1}. This can be compared with charge-transfer complexes such as hexamethylbenzene−tetracyanoethylene where the inner-sphere contribution is only 1980 cm^{-1}.[52] The larger value reorganization for the metal-to-ligand charge transfer is not unexpected given that the donor and acceptor are covalently bound in the metal complex compared to weaker intermolecular interactions that bind the donor and acceptor in the charge-transfer complexes. The strong covalent interaction between the donor and acceptor results in a larger extent of charge transfer. The largest single contribution (893 cm^{-1}) to the inner-sphere reorganization comes from the ligand acceptor mode at 1475 cm^{-1} (ν_{75}). This corresponds to a dimensionless displacement of 1.1. With the reduced mass from the normal coordinate analysis, this dimensionless displacement can be converted to a "displacement" along the normal coordinate of approximately 0.1 Å. Although this mode contains a significant contribution from bending motions, this value still gives an indication of the magnitude of the distortion resulting from the initial MLCT transition, i.e., approximately 10% of the equilibrium bond length. This relatively small change in the molecular geometry justifies the assumptions of harmonic potentials in the empirical modeling procedure. Note that the largest dimensionless displacement occurs for the quinoxaline-centered mode (ν_{29}) at 529 cm^{-1}, with a value of 1.5 in dichloromethane, and this value corresponds to a displacement of 0.15 Å.

III.e. Structure of the MLCT State. The resonance Raman excitation profile yields dimensionless displacements (Δ) that may be related to the distortion of the complex upon photoexcitation to the MLCT excited state. Those bands that show the largest Δ values lie at 1541, 1476, 1373, 1007, 749, 619, and 527 cm^{-1}. These correspond to calculated modes predicted (mode number) at 1548 (ν_{77}), 1478 (ν_{75}), 1374 (ν_{71}), 1009 (ν_{50}), 781 (ν_{39}), 648 (ν_{33}), and 538 (ν_{29}) cm^{-1}. The most striking enhancement observed in the spectrum of $[Cu(pqx)(PPh_3)_2]^+$ is the band observed at 529 cm^{-1}, this is assigned as a quinoxaline mode (ν_{29}, $0.2r_{19} + 0.15r_{10} + 0.1r_{15}$) (Figure 4). ν_{33} is a Cu−N stretch, ν_{39} also has considerable Cu−N character ($0.3r_{18} + 0.2r_{14} - 0.3r_{19} + 0.2r_{15}$). Displacements along the Cu−N coordinates are consistent with the change in oxidation state of the copper center from +1 in the ground state to +2 in the MLCT excited state. The Cu(I) geometry is tetrahedral but the Cu(II) oxidation state is 5 or 6 coordinate. The tendency of the copper center to expand its coordination sphere upon photoexcitation is well-documented in studies of the solvent-induced exciplex quenching of the MLCT excited state.[53] The resonance Raman intensity analysis confirms that some distortion of the tetrahedral copper geometry is occurring within the Franck−Condon region.

An examination of the shape of the LUMO in $Cu(pqx)(PH_3)_2^+$ would suggest that transitions involving the population of this MO, which is predicted for both LC and MLCT transitions, should lead to bonding changes about the ligand structure. This MO is antibonding across r_1, r_2, r_4, r_6, r_8, r_9, r_{11}, r_{13}, r_{15}, r_{19}, and r_{20} and bonding across r_3, r_5, r_7, r_{10}, r_{12}, r_{14}, and r_{18}.

IV. Conclusions

Understanding the magnitude and distribution of the reorganization energy between the inner sphere and outer sphere has important implications for the design of efficient charge-transfer processes in devices containing metal polypyridyl complexes. Resonance Raman intensity analysis of an MLCT transition in

a metal polypyridyl complex in polar organic solvents has demonstrated the inner-sphere contribution is similar in magnitude to the outer-sphere contribution to the total reorganization energy. For charge-transfer processes with little or no driving force the rate of charge transfer is maximized by reducing the magnitude of the total reorganization energy. The solvent reorganization energy is minimized by selecting nonpolar solvents, and the inner-sphere reorganization can be minimized by delocalizing the electron and hole during the charge-transfer process. The efficiency of the charge-transfer process is also determined by the strength of electronic coupling between the donor and acceptor, and electronic coupling may need to be traded for smaller reorganization to find an optimum charge-transfer rate. Ab initio calculations of the normal modes allows the resonance Raman data to be interpreted in terms of the geometry changes induced by charge transfer and provides a method for improving the rational design of materials with improved charge-transfer properties. An extension of this approach is to the ab initio calculation of the resonance Raman intensities themselves,[54−56] and we are directing our current efforts in this direction.

Acknowledgment. M.R.W. thanks the Royal Society of New Zealand for the award of a Fast-Start Marsden Grant (02-MAU-211). We thank the Foundation for Research Science and Technology and the MacDiarmid Institute for financial support of this work. We thank Timothy Simpson for preparing the pqx ligand and Cushla McGoverin for preparing the [Cu(pqx)-$(PPh_3)_2]^+$ complex.

Supporting Information Available: Tables of simulated and experimental resonance Raman cross-sections for Cu(pqx)-$(PPh_3)_2^+$ in dichloromethane and chloroform solutions are available as supplementary information. Crystallographic data is also available in .cif format. This material is available free of charge via the Internet at http://pubs.acs.org.

References and Notes

(1) Baldo, M. A.; O'Brien, D. F.; You, Y.; Shoustikov, A.; Sibley, S.; Thompson, M. E.; Forrest, S. R. *Nature (London)* **1998**, *395*, 151.

(2) Baldo, M. A.; Thompson, M. E.; Forrest, S. R. *Nature (London)* **2000**, *403*, 750.

(3) Baldo, M. A.; Thompson, M. E.; Forrest, S. R. *Pure Appl. Chem.* **1999**, *71*, 2095.

(4) Lamansky, S.; Djurovich, P.; Murphy, D.; Abdel-Razzaq, F.; Lee, H.-E.; Adachi, C.; Burrows, P. E.; Forrest, S. R.; Thompson, M. E. *J. Am. Chem. Soc.* **2001**, *123*, 4304.

(5) Lamansky, S.; Djurovich, P.; Murphy, D.; Abdel-Razzaq, F.; Kwong, R.; Tsyba, I.; Bortz, M.; Mui, B.; Bau, R.; Thompson, M. E. *Inorg. Chem.* **2001**, *40*, 1704.

(6) Lamansky, S.; Kwong, R. C.; Nugent, M.; Djurovich, P. I.; Thompson, M. E. *Org. Electron.* **2001**, *2*, 53.

(7) Brooks, J.; Babayan, Y.; Lamansky, S.; Djurovich, P. I.; Tsyba, I.; Bau, R.; Thompson, M. E. *Inorg. Chem.* **2002**, *41*, 3055.

(8) Klein, C.; Nazeeruddin Md, K.; Di Censo, D.; Liska, P.; Gratzel, M. *Inorg. Chem.* **2004**, *43*, 4216.

(9) Nazeeruddin, M. K.; Graetzel, M. Conversion and storage of solar energy using dye-sensitized nanocrystalline TiO_2 cells. In *Comprehensive Coordination Chemistry II*; Ward, M. D., Ed.; Elsevier Ltd: Oxford, U.K., 2004; Vol. 9, p 719.

(10) Nazeeruddin, M. K.; Humphry-Baker, R.; Officer, D. L.; Campbell, W. M.; Burrell, A. K.; Graetzel, M. *Langmuir* **2004**, *20*, 6514.

(11) Wang, P.; Klein, C.; Moser, J.-E.; Humphry-Baker, R.; Cevey-Ha, N.-L.; Charvet, R.; Comte, P.; Zakeeruddin, S. M.; Graetzel, M. *J. Phys. Chem. B* **2004**, *108*, 17553.

(12) Nazeeruddin, M. K.; Zakeeruddin, S. M.; Humphry-Baker, R.; Gorelsky, S. I.; Lever, A. B. P.; Gratzel, M. *Coord. Chem. Rev.* **2000**, *208*, 213.

(13) Barbara, P. F.; Ratner, M. A.; Meyer, T. J. *J. Phys. Chem.* **1996**, *100*, 13148.

(14) Li, B.; Johnson, A. E.; Mukamel, S.; Myers, A. B. *J. Am. Chem. Soc* **1994**, *116*, 11039.

(15) Myers, A. B. *Chem. Rev.* **1996**, *96*, 911.

(16) Streiff, J.; McHale, J. L. *J. Chem. Phys.* **2000**, *112*, 841.

(17) Doorn, S. K.; Hupp, J. T. *J. Am. Chem. Soc.* **1989**, *111*, 1142.

(18) Leung, K. H.; Phillips, D. L.; Che, C.-M.; Miskowski, V. M. *J. Raman Spectrosc.* **1999**, *30*, 987.

(19) Cheng, Y. F.; Phillips, D. L.; He, G. Z.; Che, C. M.; Chi, Y. *Chem. Phys. Lett.* **2001**, *338*, 308.

(20) Leung, K. H.; Phillips, D. L.; Mao, Z.; Che, C.-M.; Miskowski, V. M.; Chan, C.-K. *Inorg. Chem.* **2002**, *41*, 2054.

(21) Diaz-Acosta, I.; Baker, J.; Cordes, W.; Pulay, P. *J. Phys. Chem. A* **2001**, *105*, 238.

(22) Liu, J.; Mei, W. J.; Lin, L. J.; Zheng, K. C.; Chao, H.; Yun, F. C.; Ji, L. N. *Inorg. Chim. Acta* **2004**, *357*, 285.

(23) Mei, W. J.; Liu, J.; Zheng, K. C.; Lin, L. J.; Chao, H.; Li, A. X.; Yun, F. C.; Ji, L. N. *Dalton Trans.* **2003**, 1352.

(24) Xu, H.; Zheng, K.-C.; Chen, Y.; Li, Y.-Z.; Lin, L.-J.; Li, H.; Zhang, P.-X.; Ji, L.-N. *Dalton Trans.* **2003**, 2260.

(25) Zheng, K.; Wang, J.; Shen, Y.; Kuang, D.; Yun, F. *J. Phys. Chem. A* **2001**, *105*, 7248.

(26) Zheng, K.; Wang, J.; Peng, W.; Liu, X.; Yun, F. *J. Phys. Chem. A* **2001**, *105*, 10899.

(27) Zheng, K.; Wang, J.; Shen, Y.; Peng, W.; Yun, F. *J. Comput. Chem.* **2002**, *23*, 436.

(28) Zheng, K. C.; Wang, J. P.; Peng, W. L.; Shen, Y.; Yun, F. C. *Inorg. Chim. Acta* **2002**, *328*, 247.

(29) Dattelbaum, D. M.; Omberg, K. M.; Schoonover, J. R.; Martin, R. L.; Meyer, T. J. *Inorg. Chem.* **2002**, *41*, 6071.

(30) Dattelbaum, D. M.; Martin, R. L.; Schoonover, J. R.; Meyer, T. J. *J. Phys. Chem. A* **2004**, *108*, 3518.

(31) Dattelbaum, D. M.; Omberg, K. M.; Hay, P. J.; Gebhart, N. L.; Martin, R. L.; Schoonover, J. R.; Meyer, T. J. *J. Phys. Chem. A* **2004**, *108*, 3527.

(32) Howell, S. L.; Gordon, K. C. *J. Phys Chem. A* **2004**, *108*, 2536.

(33) Yam, V. W.-W.; Lo, K. K.-W. *J. Chem. Soc., Dalton Trans.* **1995**, 499.

(34) Barron, P. F.; Dyason, J. C.; Engelhardt, L. M.; Healy, P. C.; White, A. H. *Aust. J. Chem.* **1985**, *38*, 261.

(35) Shriver, D. F.; Dunn, J. B. R. *Appl. Spectrosc.* **1974**, *28*, 319.

(36) McCreery, R. L. *Raman Spectroscopy for Chemical Analysis*; John Wiley & Sons: New York, 2000.

(37) The ASTM subcommittee on Raman spectroscopy has adopted eight materials as Raman shift standards (ASTM E 1840). The band wavenumbers for these standards are available at: http://chemistry.ohio-state.edu/~rmccreer/shift.html.

(38) Myers, A. B.; Li, B.; Ci, X. *J. Chem. Phys.* **1988**, *8*, 1876.

(39) Egolf, D. S.; Waterland, M. R.; Kelley, A. M. *J. Phys. Chem. B* **2000,** *104*, 10727.

(40) Foster, C. E.; Barham, B. P.; Reid, P. J. *J. Chem. Phys.* **2001**, *114*, 8492.

(41) Lee, S.-Y.; Heller, E. J. *J. Chem. Phys.* **1979**, *71*, 4777.

(42) Tannor, D. J.; Heller, E. J. *J. Chem. Phys.* **1982**, *77*, 202.

(43) (a) Myers, A. B.; Mathies, R. A. Resonance Raman intensities: A probe of excited-state structure and dynamics. In *Biological Applications of Raman Spectroscopy*; Spiro, T. G., Ed.; Wiley: New York, 1987; Vol. 2, pp 1−58. (b) Myers, A. B. Excited electronic state properties from ground-state resonance Raman intensities. In *Laser Techniques in Chemistry*; Myers, A. B., Rizzo, T. R., Eds.; Wiley: New York, 1995; pp 325−384.

(44) Frisch, M. J.; Trucks, G. W.; Schlegel, H. B.; Scuseria, G. E.; Robb, M. A.; Cheeseman, J. R.; Montgomery, J. A., Jr.; Vreven, T.; Kudin, K. N.; Burant, J. C.; Millam, J. M.; Iyengar, S. S.; Tomasi, J.; Barone, V.; Mennucci, B.; Cossi, M.; Scalmani, G.; Rega, N.; Petersson, G. A.; Nakatsuji, H.; Hada, M.; Ehara, M.; Toyota, K.; Fukuda, R.; Hasegawa, J.; Ishida, M.; Nakajima, T.; Honda, Y.; Kitao, O.; Nakai, H.; Klene, M.; Li, X.; Knox, J. E.; Hratchian, H. P.; Cross, J. B.; Bakken, V.; Adamo, C.; Jaramillo, J.; Gomperts, R.; Stratmann, R. E.; Yazyev, O.; Austin, A. J.; Cammi, R.; Pomelli, C.; Ochterski, J. W.; Ayala, P. Y.; Morokuma, K.; Voth, G. A.; Salvador, P.; Dannenberg, J. J.; Zakrzewski, V. G.; Dapprich, S.; Daniels, A. D.; Strain, M. C.; Farkas, O.; Malick, D. K.; Rabuck, A. D.; Raghavachari, K.; Foresman, J. B.; Ortiz, J. V.; Cui, Q.; Baboul, A. G.; Clifford, S.; Cioslowski, J.; Stefanov, B. B.; Liu, G.; Liashenko, A.; Piskorz, P.; Komaromi, I.; Martin, R. L.; Fox, D. J.; Keith, T.; Al-Laham, M. A.; Peng, C. Y.; Nanayakkara, A.; Challacombe, M.; Gill, P. M. W.; Johnson, B.; Chen, W.; Wong, M. W.; Gonzalez, C.; Pople, J. A. *Gaussian 03*, revision C.02; Gaussian, Inc.: Wallingford, CT, 2004.

(45) Schaftenaar, G.; Noordik, J. H. *J. Comput. Aided Mol. Des.* **2000**, *14*, 123.

(46) Guirgis, G. A.; Nashed, Y. E.; Durig, J. R. *Spectrochim. Acta Pt. A-Mol. Biomolec. Spectrosc.* **2000**, *56*, 1065.

(47) Guirgis, G. A.; Nashed, Y. E.; Durig, J. R. *J. Mol. Struct.* **1999**, *510*, 13.

(48) Durig, J. R.; Pan, C.; Klaeboe, P.; Aleksa, V.; Guirgis, G. A. *Spectrochim. Acta, Pt. A: Mol. Biomol. Spectrosc.* **2003**, *59A*, 2151.

(49) Veroni, I.; Rontoyianni, A.; Mitsopoulou, C. A. *Dalton Trans.* **2003**, 255.
(50) Britt, B. M.; McHale, J. L.; Friedrich, D. M. *J. Phys. Chem.* **1995**, *99*, 6347.
(51) Godbout, J. T.; Pietrzykowski, M. D.; Gould, I. R.; Goodman, J. L.; Kelley, A. M. *J. Phys. Chem. A* **1999**, *103*, 3876.
(52) Kulinowski, K.; Gould, I. R.; Myers, A. B. *J. Phys. Chem.* **1995**, *99*, 9017.
(53) Kalyanasundaram, K. *Photochemistry of Polypyridine and Porphyrin Complexes*; Academic Press Ltd: London, 1992.
(54) Hudson, B. S.; Markham, L. M. *J. Raman. Spectrosc.* **1998**, *29*, 489.
(55) Waterland, M. R.; Kelley, A. M. *J. Phys. Chem. A* **2001**, *105*, 8385.
(56) Waterland, M. R.; Stockwell, D.; Kelley, A. M. *J. Chem. Phys.* **2000**, *114*, 6249.